PAPER • OPEN ACCESS

Shock ripples observed by the MMS spacecraft: ion reflection and dispersive properties

View the article online for updates and enhancements.

IOP ebooks™

Bringing you innovative digital publishing with leading voices to create your essential collection of books in STEM research.

Start exploring the collection - download the first chapter of every title for free.

Shock ripples observed by the MMS spacecraft: ion reflection and dispersive properties

Andreas Johlander[1,2] , Andris Vaivads[1], Yuri V Khotyaintsev[1],
Imogen Gingell[3], Steven J Schwartz[3,4], Barbara L Giles[5],
Roy B Torbert[6] and Christopher T Russell[7]

[1] Swedish Institute of Space Physics, Uppsala SE-75121, Sweden
[2] Department of Physics and Astronomy, Uppsala University, Uppsala SE-75120, Sweden
[3] Imperial College London, London SW7 2AZ, United Kingdom
[4] Laboratory for Atmospheric and Space Physics, University of Colorado, Boulder, CO 80303, United States of America
[5] NASA, Goddard Space Flight Center, Greenbelt, MD 20771, United States of America
[6] University of New Hampshire, Durham, NH 03824, United States of America
[7] Earth Planetary and Space Sciences, University of California, Los Angeles, CA 90095, United States of America

E-mail: andreas.johlander@gmail.com

CrossMark

Abstract
Shock ripples are ion-inertial-scale waves propagating within the front region of magnetized quasi-perpendicular collisionless shocks. The ripples are thought to influence particle dynamics and acceleration at shocks. With the four magnetospheric multiscale (MMS) spacecraft, it is for the first time possible to fully resolve the small scale ripples in space. We use observations of one slow crossing of the Earth's non-stationary bow shock by MMS. From multi-spacecraft measurements we show that the non-stationarity is due to ripples propagating along the shock surface. We find that the ripples are near linearly polarized waves propagating in the coplanarity plane with a phase speed equal to the local Alfvén speed and have a wavelength close to 5 times the upstream ion inertial length. The dispersive properties of the ripples resemble those of Alfvén ion cyclotron waves in linear theory. Taking advantage of the slow crossing by the four MMS spacecraft, we map the shock-reflected ions as a function of ripple phase and distance from the shock. We find that ions are preferentially reflected in regions of the wave with magnetic field stronger than the average overshoot field, while in the regions of lower magnetic field, ions penetrate the shock to the downstream region.

Supplementary material for this article is available online

Keywords: shock ripples, ion reflection, ion dynamics, magnetospheric multiscale, space plasma, collisionless shocks

1. Introduction

Shock waves in collisionless plasmas are ubiquitous in the Universe. Stellar termination shocks, planetary and stellar bow shocks, and intergalactic shocks all act to slow down and thermalize supersonic plasma (Tsurutani and Stone 1985).

Collisionless shock waves are also powerful particle accelerators. Shock waves caused by the fast ejecta from supernova remnants are the most likely source of the high energy cosmic rays that permeate the galaxy (e.g. Blandford and Ostriker 1978, Morlino and Caprioli 2012). An important parameter for magnetized shock waves is the angle θ_{Bn} between the upstream magnetic field and the shock normal vector. The shock is quasi-perpendicular when $\theta_{Bn} > 45°$ and quasi-parallel when $\theta_{Bn} < 45°$. Quasi-perpendicular shock waves are characterized by a sharp and sudden deceleration of the plasma while quasi-parallel shocks have a more extended and turbulent transition between up- and downstream (Schwartz and Burgess 1991). Non-stationary shocks have unstable motion and structure despite stable upstream conditions. Both quasi-parallel and quasi-perpendicular shock waves are known to be non-stationary in simulations (e.g. Krasnoselskikh *et al* 2002, Hao *et al* 2016). There are a few types of shock non-stationarity observed in simulations (Lembege *et al* 2004). One is *self-reformation*, where a new shock front cyclically forms in the foot upstream of the old shock. Another type is *rippling*, where waves move along the shock front, which appears as non-stationary. Which type of non-stationarity is dominant depends on plasma parameters and simulation setup. Shock non-stationarity has been shown to influence the dynamics and acceleration processes of both electrons (Umeda *et al* 2009, Matsukiyo and Matsumoto 2015) and ions (Yang *et al* 2009, Caprioli *et al* 2015). There are a few *in situ* observations of shock non-stationarity in space (e.g. Moullard *et al* 2006, Lobzin *et al* 2007, Johlander *et al* 2016). However, detailed, quantitative studies on non-stationarity and its effect on particles dynamics is still lacking.

Waves in quasi-perpendicular shocks that cause magnetic field and density fluctuations are commonly observed in simulations. In 2D simulations where the magnetic field is in the simulation plane, these *shock ripples* are usually considered to be Alfvénic type waves and have been shown to influence ion and electron dynamics at the shock (Umeda *et al* 2009, Saito and Umeda 2011, Yang *et al* 2012). The first observations of shock ripples in simulations was made by Winske and Quest (1988). The authors proposed that the ripples are generated by the Alfvén ion cyclotron (AIC) instability, which is caused by an ion temperature anisotropy $T_{i,\perp} > T_{i,\parallel}$ in a high-ion beta β_i plasma (Davidson and Ogden 1975). The ion temperature anisotropy arises from the ion reflection and adiabatic compression of the transmitted ions at the shock. Winske and Quest (1988) also discusses the drift mirror instability as an alternative source of the shock ripples. Like the AIC instability, the mirror instability arises from a temperature anisotropy. When a density gradient is present the mirror wave obtains a real frequency and propagates mainly perpendicular to the magnetic field (Hasegawa 1969). Despite limitations set by linear theory and 2D simulations, Winske and Quest (1988) concluded that the shock ripples fit better to the description of AIC waves than drift mirror waves. McKean *et al* (1995) found in simulations that both AIC and drift mirror waves are generated at the shock front and convected downstream. McKean *et al* (1995) also observed nonuniform ion reflection along the shock surface. Lowe and

Burgess (2003) in detail determined the dispersive properties of the ripples and found that they propagate along the magnetic field with phase speed close to the local Alfvén speed V_A, and with a frequency of a few times the upstream ion cyclotron frequency ω_{ci}. The generation mechanism of the ripples is still poorly understood in part because of the difficulties with linear analysis at the steep gradient of the shock ramp. Gingell *et al* (2017) observed, for the first time to our knowledge, ripples in a shock with $\theta_{Bn} < 80°$ and showed that the ripples have similar dispersive properties in these more oblique and even quasi-parallel geometries. A distinctly different type of large-amplitude fluctuations in the shock observed in fully kinetic 2D simulations is a whistler branch wave that propagates obliquely to the magnetic field (Hellinger *et al* 2007, Lembège *et al* 2009). These waves are different from the previously observed shock ripples and are likely a competing mechanism for shock non-stationarity. In 2D simulations where the magnetic field is perpendicular to the simulation plane, other types of instabilities dominate at the shock. In hybrid simulations Burgess and Scholer (2007) found ripple-like structures moving in the direction and speed of gyration of the shock-reflected ions. These fluctuations were found to be linked with fluctuations in the amount of reflected ions. In 3D hybrid simulations Burgess *et al* (2016) found that the shock structure is dominated by a combination of fluctuations propagating along the magnetic field and in the direction of reflected ion gyration. Burgess *et al* (2016) also found at higher Mach numbers ($M_A = 5.5$) field-propagating ripples are the dominant feature. From simulations, it is still unclear in what parts of parameter space shock ripples are expected and exactly what role they play in plasma thermalization and acceleration.

There are a few *in situ* space observations of shock ripples from the terrestrial bow shock. Moullard *et al* (2006) found evidence for shock ripples using a slow partial shock crossing by the four Cluster spacecraft. Recently, using the four closely-spaced magnetospheric multiScale (MMS) spacecraft (Burch *et al* 2016), shock ripples have been observed at quasi-perpendicular (Johlander *et al* 2016), and marginally quasi-parallel (Gingell *et al* 2017) shocks. Despite this, there is still a lack of detailed *in situ* studies accurately determining dispersive properties and what role ripples play in ion reflection and heating. In this paper, we present observations from one event of shock rippling at the Earth's bow shock observed by the MMS spacecraft. The favorable spacecraft trajectories where MMS skim the shock front for a long time, combined with MMS's high-cadence field and plasma observations, allows for unprecedented detailed observations of the shock ripples. With the observations we characterize in detail the dispersive properties of the ripples and their impact on ion reflection at the shock.

2. Observations

2.1. The event

We study one slow partial crossing by MMS of Earth's quasi-perpendicular bow shock on the 6 January 2016, 00:33 UT.

Magnetic field data are from the fluxgate magnetometer (Russell *et al* 2016). Ion and electron data are from the fast plasma investigation (FPI) instruments dual ion/electron spectrometer, FPI-DIS and FPI-DES respectively (Pollock *et al* 2016). FPI can sample the full 3D distribution function every 150 ms for ions and 30 ms for electrons. The FPI instruments on MMS are primarily designed to make accurate measurements at the magnetopause. Plasma measurements of the cold solar wind beam may therefore be less accurate. As soon as the plasma starts being heated and slowed by the shock the plasma measurements by FPI become reliable. However, to obtain more accurate plasma parameters upstream of the shock we use ion temperature data from the solar wind experiment (Ogilvie *et al* 1995) on the Wind spacecraft that is situated upstream of MMS at Lagrange point 1. The data from Wind are time-shifted to the bow shock and provided by the OMNI database.

At the time of the event, all four MMS spacecraft experience a partial crossing of the bow shock. The spacecraft are flying in a tetrahedron formation with inter-spacecraft separations of ∼35 km. MMS1 is positioned furthest earthward and therefore reaches furthest downstream in the shock. In this paper, MMS1 will be used as the reference spacecraft. Figure 1 shows magnetic field and ion data for the event. In the figure, MMS starts out in the downstream (shocked) magnetosheath and then crosses the bow shock to the upstream (unshocked) solar wind. The bow shock then slowly moves sunward, leading to MMS encountering first the shock foot then ramp and overshoot before the shock moves back and MMS returns upstream. We adopt the naming *inbound phase* for the first half of the crossing and *outbound phase* for the later half. In the partial shock crossing, MMS never reaches the asymptotic downstream plasma as can clearly be seen when comparing to the previous shock crossing on the same day, particularly in ion density. During this almost 1 min long encounter with the shock, MMS observes large fluctuations in magnetic field and plasma parameters with a frequency of close to 0.5 Hz. As we will show below, these fluctuations are due to ripples or surface waves traversing the shock surface. Since the fluctuations are more periodic and less noisy in the outbound phase, we will focus on this period in our analysis. The goal of this paper is to study the physical properties of the shock ripples. Since this partial shock crossing is particularly slow, MMS observes many ripple periods, which allows for detailed analysis of fluctuations and their impact on ion dynamics and reflection.

Our analysis of the shock requires an accurate determination of the shock normal vector. The inter-spacecraft separation is smaller than the scale of the ripples and the shock crossing is relatively slow. This means that it is impossible to perform four-spacecraft timing on the overall shock structure for a determination of the shock normal vector $\hat{\mathbf{n}}$. Since the shock crossing is partial, MMS never reaches the asymptotic downstream plasma, and therefore mixed mode methods using up- and downstream plasma values (Abraham-Shrauner 1972) are also inapplicable. Instead, we employ a bow shock model (Slavin and Holzer 1981, Schwartz 1998), fitted to the spacecraft position to calculate $\hat{\mathbf{n}}$. The shock
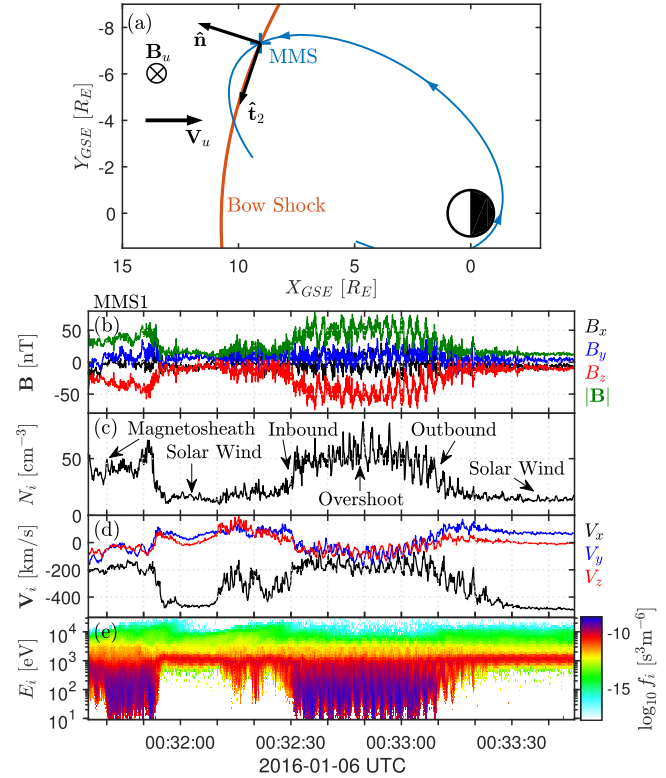

Figure 1. Overview of the event observed by MMS1. (a) Orbit (line) and shock crossing (+) of MMS in blue in geocentric solar ecliptic (GSE) coordinates in Earth radii R_E. Bow shock model from (Slavin and Holzer 1981) is shown as a red line. Indicated are also approximate directions of upstream flow velocity $\mathbf{V}_u$, and magnetic field $\mathbf{B}_u$, as well as the coordinate vectors $\hat{\mathbf{n}}$ and $\hat{\mathbf{t}}_2$. (b) Magnetic field in GSE coordinates. (c) Ion number density with arrows indicating in which region of the shock MMS is at different times. (d) Ion flow velocity in GSE coordinates. (e) Ion phase-space density energy distribution.

speed on the outbound side of the shock crossing in the spacecraft frame was determined using the shock foot thickness method by Gosling and Thomsen (1985) using a foot crossing time of 30s. The resulting normal vector and shock speed are presented in table 1. The acute angle between the shock normal and upstream magnetic field θ_{Bn} is ∼64° measured immediately after the crossing, and ∼60° measured right before the crossing. The measurement right before the crossing has larger uncertainty in θ_{Bn} due to larger **B** fluctuations. From now on we assume that the shock angle is ∼64° and remains constant throughout the shock crossing.

We use the normal incidence (NI) frame to facilitate comparison to simulations. In the NI frame, the incoming upstream plasma travels along the shock normal, and the shock itself is at rest. The shock aligned coordinate system we use in our analysis is based on $\hat{\mathbf{n}}$ and the average upstream magnetic field $\mathbf{B}_u$. We define $\hat{\mathbf{t}}_2 = \hat{\mathbf{n}} \times \mathbf{B}_u / |\hat{\mathbf{n}} \times \mathbf{B}_u|$ and $\hat{\mathbf{t}}_1 = \hat{\mathbf{t}}_2 \times \hat{\mathbf{n}}$ completes the right-handed (n, t_1, t_2) system. Now, $n - t_1$ is the coplanarity plane and $\hat{\mathbf{t}}_2$ is the out-of-plane direction and is close to the direction of the upstream convection electric field, see figure 1.

Table 1. Shock and plasma parameters. The subscript *u* denotes upstream or unshocked values. Upstream parameters are measured after the shock crossing unless otherwise stated. The Mach numbers are calculated in the normal incidence frame.

Parameter	Value
Magnetic field magnitude B_u	12 nT
Solar wind density N_u	12 cm^{-3}
Solar wind speed V_u	500 km s^{-1}
Alfvén Mach number M_A	7
Magnetosonic Mach number M_{ms}	5
Solar wind ion $\beta_{i,u}$	0.6
Shock normal $\hat{\mathbf{n}}$ in GSE	(0.95, −0.30, −0.05)
$\hat{\mathbf{t}}_1$ in GSE	(0.03, 0.24, −0.97)
$\hat{\mathbf{t}}_2$ in GSE	(0.33, 0.92, 0.24)
Shock speed, outbound phase V_{sh}	4 km s^{-1}
Shock normal angle θ_{Bn}	64 ± 6°
θ_{Bn} before crossing	60 ± 25°
Ion inertial length $d_{i,u}$	61 km
Ion gyrofrequency $f_{ci,u}$	0.2 Hz
Alfvén speed in overshoot, $v_{A,o}$	140 km s^{-1}

2.2. The non-stationary shock

The strong fluctuations observed throughout the shock crossing suggests that the shock is non-stationary. Here we investigate the nature of the non-stationarity. The major competing non-stationarity processes in this case are the shock self-reformation (e.g. Lembège and Savoini 1992, Lobzin *et al* 2007) and shock rippling (e.g. Winske and Quest 1988, Johlander *et al* 2016). Simultaneous measurements at four different points in the shock can help us to determine whether the shock undergoes self-reformation or is rippled. Figure 2(b) shows ∇B calculated from four-spacecraft measurements (Chanteur 1998). In the case of a continuous and laminar shock, one would expect to see the shock ramp as a single gradient increase with $\nabla B \cdot \hat{\mathbf{n}} < 0$. As can be seen in figure 2(b), we observe several peaks in ∇B. In the case of self-reformation, a new shock front is formed upstream of the shock ramp and then convects downstream, past the spacecraft. An example of 2D simulations with clear reformation signatures can be seen in figures 2(a) and 3 in Lembège and Savoini (2002). In this case, one would expect that $\nabla B \cdot \hat{\mathbf{n}}$ should show significant positive values in the shock foot when the new shock ramp convects past MMS. These positive values are expected to be comparable in magnitude to the negative values in the ramp. However, as can be seen in figure 2(b) $\nabla B \cdot \hat{\mathbf{n}}$ is dominantly negative throughout the shock foot. If instead the shock is rippled, the shock is similar to a continuous and laminar shock, but with a wave-like structure of the surface. In this case, $\nabla B \cdot \hat{\mathbf{n}}$ is also expected to be mainly negative in the shock foot and ramp, in agreement with observations. The fluctuations in $\nabla B \cdot \hat{\mathbf{n}}$ can be explained by the shock ramp repeatedly moving up- and downstream relative to MMS due to the rippling. Since the ripples exist in the gradient of the shock ramp, $\nabla B \cdot \hat{\mathbf{n}}$ would not necessarily be positive even if the ripple phase speed has a component downstream. The slightly positive values close to

the overshoot are likely because MMS1 reaches the downstream edge of the overshoot and therefore observes a lower B. The behavior of mainly negative gradient in the shock foot is validated by gradients of electron density and temperature (not shown). In addition, as we shall see below, four-spacecraft observations also show that the fluctuations propagate with a large component in the tangential direction i.e. along the shock surface. Thus, we conclude that the multipoint observations from within the shock clearly favor ripples over self-reformation.

We also study the ion dynamics to investigate the non-stationarity mechanism. Figures 2(c)–(g) shows reduced ion phase-space density along the three principal velocity directions $\hat{\mathbf{n}}$, $\hat{\mathbf{t}}_1$, and $\hat{\mathbf{t}}_2$. The ion phase-space density f_i is integrated along the other two velocity directions so that $F_i(V_1) = \int f_i(\mathbf{V})\mathrm{d}V_2\,\mathrm{d}V_3$. Panel (c) shows the full ion distribution as a function of V_n in the spacecraft frame. The speed of the NI frame $\mathbf{V}_{NI} \cdot \hat{\mathbf{n}} = V_{sh}$ is marked with a dashed line. In the following panels, we only show partial distributions corresponding to $V_n < V_{sh}$ for incident ions and $V_n > V_{sh}$ for reflected ions. We can make several important observations in figure 2. First, there are phase-space hole-like structures in V_n and periodic variability in the amount of reflected ions. Similar behavior is expected from simulations both of self-reformation (Lembège and Savoini 1992) and of ripples (McKean *et al* 1995). In both cases, the phase-space holes are due to the spacecraft periodically moving between the thermalized shocked downstream plasma and the upstream plasma, which is characterized by counter-streaming solar wind and shock reflected ion populations. Secondly, as can be seen in figure 2(d), the incident solar wind exhibits large fluctuations in V_{t1}. From the Rankine–Hugoniot relations (Landau and Lifshitz 1960), we find that the change in V_{t1} from up- to downstream should be $\sim$10 km s^{-1}. Any fluctuations arising from a change in shock strength (as in self-reformation) would be of this order. However, the observed fluctuations in V_{t1} are $>$100 km s^{-1}, clearly greater than expected for self-reformation. The V_{t1} fluctuations can however be explained by local changes in $\hat{\mathbf{n}}$ due to shock ripples. To estimate the magnitude of the fluctuations from this effect, we assume the Rankine–Hugoniot relations are locally fulfilled in a rippled shock. This assumption is approximative since shock ripples is smaller than the fluid scales required for the Rankine–Hugoniot relations. We find that a relatively small turning of $\sim$10° in $\hat{\mathbf{n}}$ can explain the observed velocity fluctuations. Also the reflected ion velocity fluctuates greatly in V_{t1}, consistent with near-specular ion reflection of a shock surface that is periodically turning due to ripples. In figures 2(f)–(g) in the outbound shock foot, we can see the solar wind and reflected ions with large positive V_{t2}. Further downstream, the solar wind fluctuates in V_{t2} due to a variability in the amount of reflected ions that together with the solar wind gyrate around the common center of momentum. The variability in reflected ions can clearly be seen in figure 2(g). A large portion of these reflected ions turn around before they reach upstream to the foot, see panel (f). Overall,
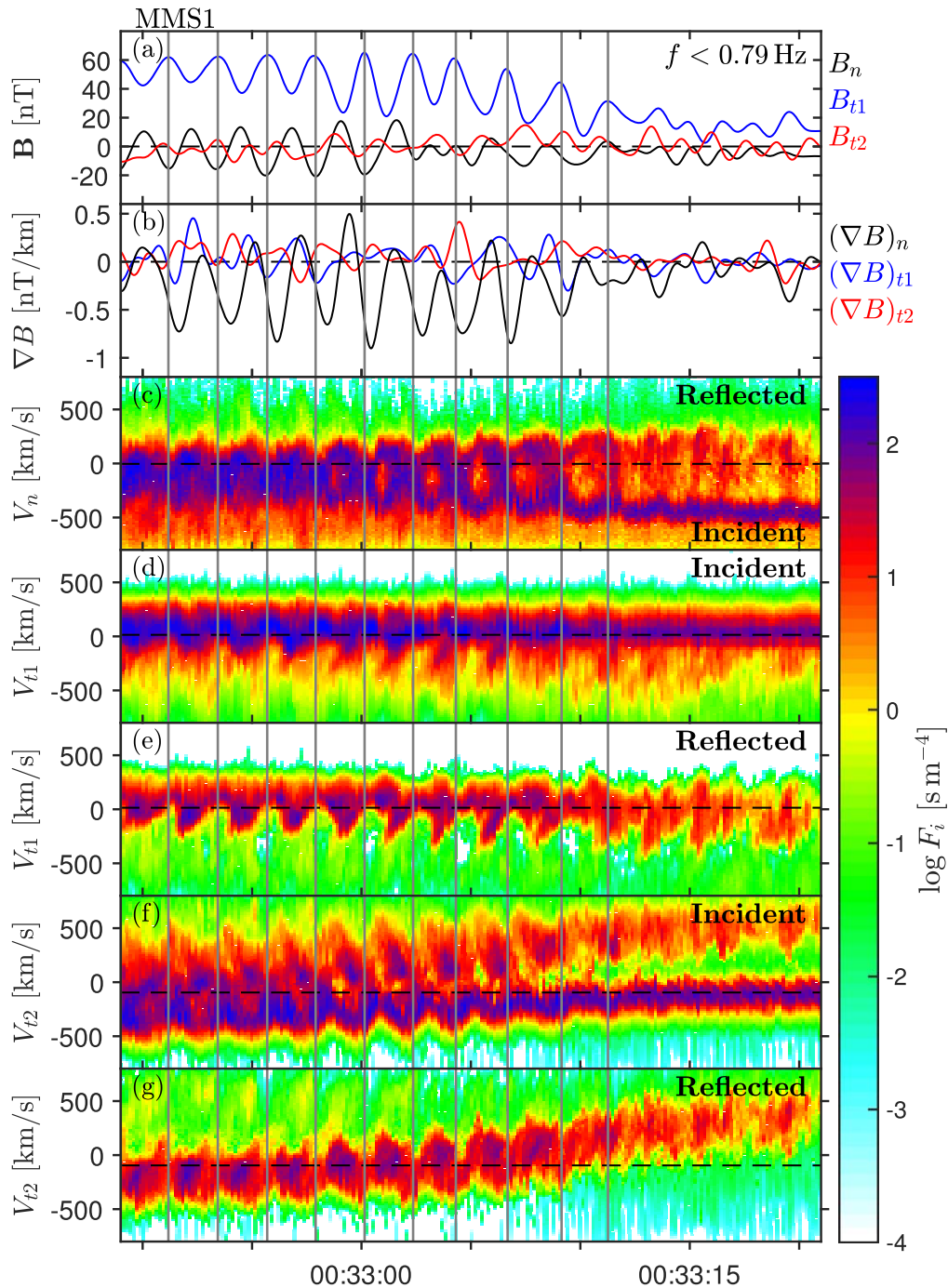
Figure 2. Magnetic field and ion phase-space density for MMS1. (a) Low-pass filtered magnetic field in shock aligned coordinates. Times where the B peaks are marked by vertical lines in all panels. (b) Gradient of B using measurements from all four MMS spacecraft. (c) The full ion distribution as a function of V_n measured by MMS1, integrated along the other two directions. The dashed line indicates the speed of the NI frame. The part of the distribution above the dashed line we call incident and the part above the line we call reflected. We use this simple separation for illustrative purposes only. (d)–(g) Partial ion distributions as a function of V_{t1} and V_{t2} showing the incident and reflected populations separately.

the ion distribution functions in figure 2 support the case of non-stationarity in the form of shock ripples.

2.3. Dispersive properties

The ripples appear as quasi-periodic waves in the shock overshoot. Here, we determine the dispersive properties of these waves. The phase speed and direction of propagation, $\hat{\mathbf{k}}$ is determined using timing analysis of low-pass filtered B_n from all four spacecraft. We use the timing method by Vogt *et al* (2011), which also gives error estimates of speed and propagation direction. Figure 3(a) shows B_n for all four MMS spacecraft as well as the time interval used in the timing. Figure 3(b) also shows B_n time-shifted so that the mean square
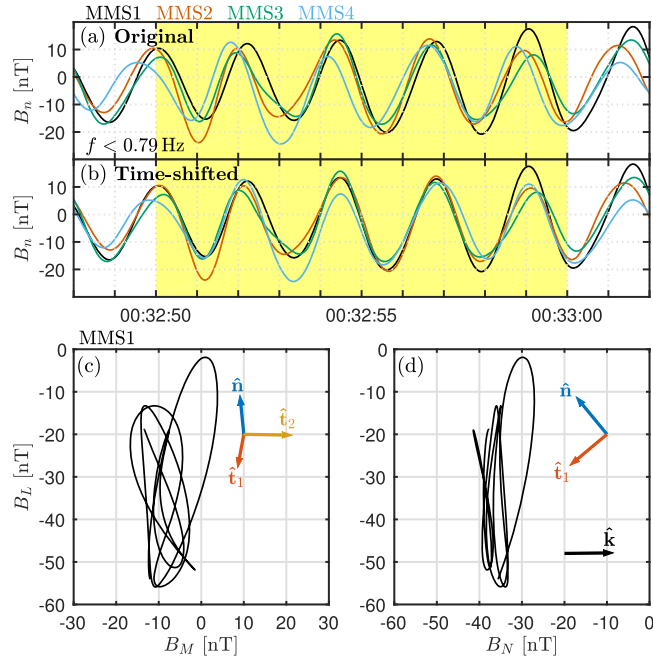
Figure 3. Results from timing and minimum variance analyzes. (a) B_n as a function of time for all four MMS spacecraft. The time interval used for both timing and minimum variance analyzes is indicated in yellow. (b) B_n for all four spacecraft but shifted in time to minimize the difference in signals. (c) **B** along intermediate and maximum variance vectors. (d) **B** along minimum and maximum variance vectors. The shock aligned coordinate system and $\hat{\mathbf{k}}$ from timing is indicated in (c) and (d).

deviation between the signals is minimized. The resulting phase speed in the spacecraft frame is $133 \pm 12 \, \mathrm{km \, s^{-1}}$ and $\hat{\mathbf{k}} = (-0.63, -0.78, 0.00)$ in shock aligned coordinates (n, t_1, t_2) with an angular uncertainty of $\sim7°$. The timing shows that the waves propagate almost entirely in the coplanarity plane. The phase speed in the NI frame is $144 \pm 23 \, \mathrm{km \, s^{-1}}$ or $1.0 \pm 0.2 V_{A,o}$, where $V_{A,o}$ is the local Alfvén speed in the overshoot. Furthermore, the angle between the local background magnetic field and propagation θ_{kB} is $42 \pm 7°$. In the spacecraft frame the frequency f^{SC} is $0.46 \pm 0.04 \, \mathrm{Hz}$, where the errors are the FWHM of the peak of the ripples in Fourier-space. In the NI frame, the frequency is $f^{\mathrm{NI}} = 0.50 \pm 0.04 \, \mathrm{Hz}$ or $2.8 \pm 0.2 f_{ci,u}$. This yields a wavelength of $\lambda = 290 \pm 40 \, \mathrm{km}$ or $4.7 \pm 0.6 d_{i,u}$. Overall, the dispersive properties are in good agreement with those observed in 2D and 3D hybrid simulations (Lowe and Burgess 2003, Ofman and Gedalin 2013, Burgess *et al* 2016), and previous *in situ* observations, (Johlander *et al* 2016, Gingell *et al* 2017).

The observations show that the shock ripples propagate only in one direction. In our case the projection of wave vector is anti-parallel to an average magnetic field direction. In simulations, it is commonly observed that the waves propagate at the same time parallel and antiparallel to **B** (Lowe and Burgess 2003, Burgess *et al* 2016, Lee 2017). We note however that the simulations were performed with θ_{Bn} close to $90°$ and that the smaller shock angle in the observations could be the cause for the symmetry breaking of wave propagation direction. In a recent simulation, Gingell *et al*

(2017) observed shock ripples that propagated along **B**. However, in the simulations, the upstream magnetic field is pointing away from the shock, $\mathbf{B}_u \cdot \hat{\mathbf{n}} > 0$, and one might therefore expect a different direction of propagation. What determines the preferred propagation direction remains an open question and requires further investigation.

The polarization of the ripples provides important information on magnetic structure and wave mode of the ripples. We therefore perform a minimum variance analysis (MVA) (Sonnerup and Scheible 1998) using the magnetic field. For the MVA, we use **B** measured by MMS1 in the time interval shown in figures 3(a), (b) band-pass filtered between 0.27 and 0.79 Hz. The resulting minimum variance vector, $\hat{\mathbf{N}}$, is within $10°$ from $\hat{\mathbf{k}}$, in reasonable agreement with the timing analysis. It is also clear that the waves are nearly linearly polarized. Figures 3(c), (d) shows hodograms of **B** in the minimum N, intermediate M, and maximum L variance directions. The eigenvalue ratio between the maximum and intermediate variance vectors is ~13. The direction of $\hat{\mathbf{L}}$ is nearly perpendicular to $\hat{\mathbf{t}}_2$. These observations show that in addition to propagating in the coplanarity plane, the magnetic field fluctuations are also in this plane in the form of linearly polarized ripples.

2.4. Ion reflection off a rippled shock

Here, we in detail analyze how ion reflection depends on the phase of the ripples and on distance to the shock. In order to do this, we divide the shock into phase bins based on **B** fluctuations. Due to the quasi-periodic behavior of the waves, the phase bins are picked by hand based on the low-pass filtered B for each spacecraft. The phase $\varphi = 0°$ is defined as the local maximum of B and $\varphi = 180°$ as the local minimum of B. The bin width is set to $60°$, and the rest of the bins are equally spaced between the $0°$- and $180°$-bins. The time intervals defined for all four spacecraft for every bin are shown in figure 4. After being divided into bins given the phase of the ripples, the data can be further divided into bins defined by the distance along the shock normal. We do this by assuming a constant overall motion of the shock in the normal direction. The time of an observation can then be transformed to distance from the shock. The width of these bins is set to 20 km. By assuming a constant wavelength of the ripples, we can further transform phase into tangential distance along the shock surface. This allows us to create maps of the shock in the $n - t_1$ plane. An example of such a map is shown in figure 5(a) where the color denotes the average value of all measurements of B by any spacecraft in each bin. In the figure, the data is repeated two times side-by-side. Bins are slanted since the ripples propagate $\sim40°$ downstream with respect to the shock surface. A constant wave phase φ then translates to a line $t_1 = -n k_n / k_{t1} + \varphi \lambda / 2\pi$. Also included in figure 5(a) are magnetic field lines constructed from the observed B_n and B_{t1}. For the field lines, we enforce $\nabla \cdot \mathbf{B} = 0$ while preserving the field as close as possible to the original. This does however mean that the B_n fluctuations are somewhat exaggerated in the field lines, likely due to the exclusion of B_{t2}. The magnetic field lines showing the
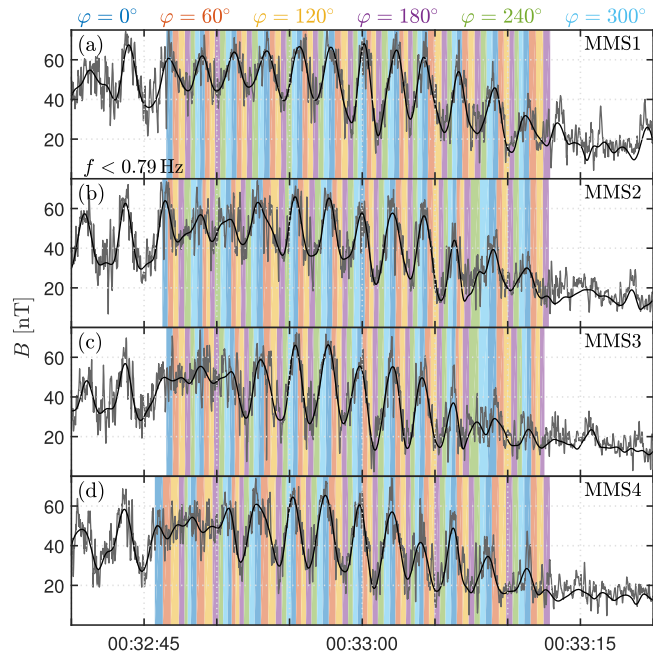
Figure 4. Magnetic field magnitude and the phase bins for all four MMS spacecraft. Full resolution B is shown as gray lines with the low-pass filtered B is overlaid as a black line. The phase bins for the individual spacecraft are shown as colored bars. The phase corresponding to the bin center for each bin is shown at the top.

structure of the ripples together with the maps of different physical parameters are helpful tools when analyzing the ripples.

Next, we investigate how ions are reflected in the shock. We have previously seen that ion reflection is highly variable in time. To determine how this translates to spatial variations we construct a map showing the density of ions that are moving upstream away from the shock, $N_{i,r}$. Most of the reflected ions after a gyration will be moving downstream towards the shock, which can be seen in figure 2(f) as incident ions with high positive values of V_{t2}. Thus, $N_{i,r}$ can be considered as the density of newly reflected ions that are between the point of reflection and the turnaround point. The map is shown in figure 5(b). The figure shows that the density of reflected ions is phased by the ripples and the highest density of reflected ions is observed in the region with the lowest magnetic field. Further upstream $N_{i,r}$ is displaced in the positive t_1 direction. This is a clear indication that ion reflection is much more efficient in localized regions of the ripples.

The observed ion distribution functions indicate that ions are being reflected in regions of high B. Ion projections for two representative times are shown in figures 5(c)–(f). Here, F_i is the integrated phase-space density along the out-of-plane velocity component. The distribution in figures 5(c)–(d) is from a region with high B. Here, the solar wind is strongly heated and deflected and a part of the distribution has started to turn around to the upstream. The distribution in figures 5(e)–(f) is from a time with low B. Here instead the incoming solar wind is colder than in the previous case and less deflected. At the same time we see a relatively cold beam

of reflected ions. The incoming solar wind and reflected populations are clearly separated in velocity space indicating that ion reflection is not occuring in this region. Instead, these ions were reflected in another part of the rippled shock because the reflected has positive V_{t1} and that the ripples move in the negative t_1-direction. We have drawn two approximate ion trajectories in figure 5(b) that explains the observed ion distributions. In the high-B region, the solar wind is slowed down and reflected. In the low-B region, the solar wind is relatively undisturbed, while at the same time ions reflected from the high-B region are observed here due to the motion of the ripples.

3. Discussion

Shock ripples are often considered to be Alfvénic type waves. In simulation work, the shock ripples are often explained by the AIC instability by an ion temperature anisotropy (e.g. Winske and Quest 1988, Burgess *et al* 2016, Lee 2017). This reasoning is done by comparison between the simulation results and linear homogeneous theory. Here, we compare the *in situ* observations to wave modes from the numerical dispersion relation solver waves in homogeneous anisotropic magnetized plasma (WHAMP) (Rönnmark 1982). WHAMP does assume small amplitude waves in homogeneous plasma and in the setup we assume a single anisotropic Maxwellian ion distribution. These assumptions are unfulfilled for the non-linear ripples that propagate in the steep gradient of the shock ramp. This means that the results from this analysis should be considered approximative and can in the best case hint at the true nature of the waves. However, a more thorough theoretical description is outside the scope of this work. We use WHAMP to find dispersion relations for the Alfvén and the whistler branches in order to differentiate between the fluctuations observed in (e.g. Winske and Quest 1988) and (Hellinger *et al* 2007, Lembège *et al* 2009). The real and imaginary parts of the frequencies ω as a function wave number k for the two branches are shown in figure 6. For the calculations, we use plasma parameters measured by MMS in the overshoot and a propagation angle $\theta_{kB} = 42°$. The dispersion relations show that the whistler mode is damped for these parameters while Alfvén waves have a positive growth rate due to the temperature anisotropy.

We now compare the theoretical wave modes to the observed dispersive properties of the shock ripples. To further study the dispersive properties we need the wave properties in the local plasma (LP) frame, which is defined be averaged values of $\mathbf{V}_i$ in the overshoot. In the LP frame, the frequency is 0.29 ± 0.05 Hz and the phase speed is 82 ± 19 km s^{-1}, see figure 6. Despite the caveats about nonlinearity and inhomogeneity, we note that the ripples closely resemble Alfvén waves. The ripples are observed at the wave number where the growth rate for AIC instability is positive. Furthermore, the observed frequency is a rather good match to that given by WHAMP for Alfvén waves. We also observe that the ripples are linearly polarized which is also the case for oblique Alfvén waves in WHAMP. For the observed plasma
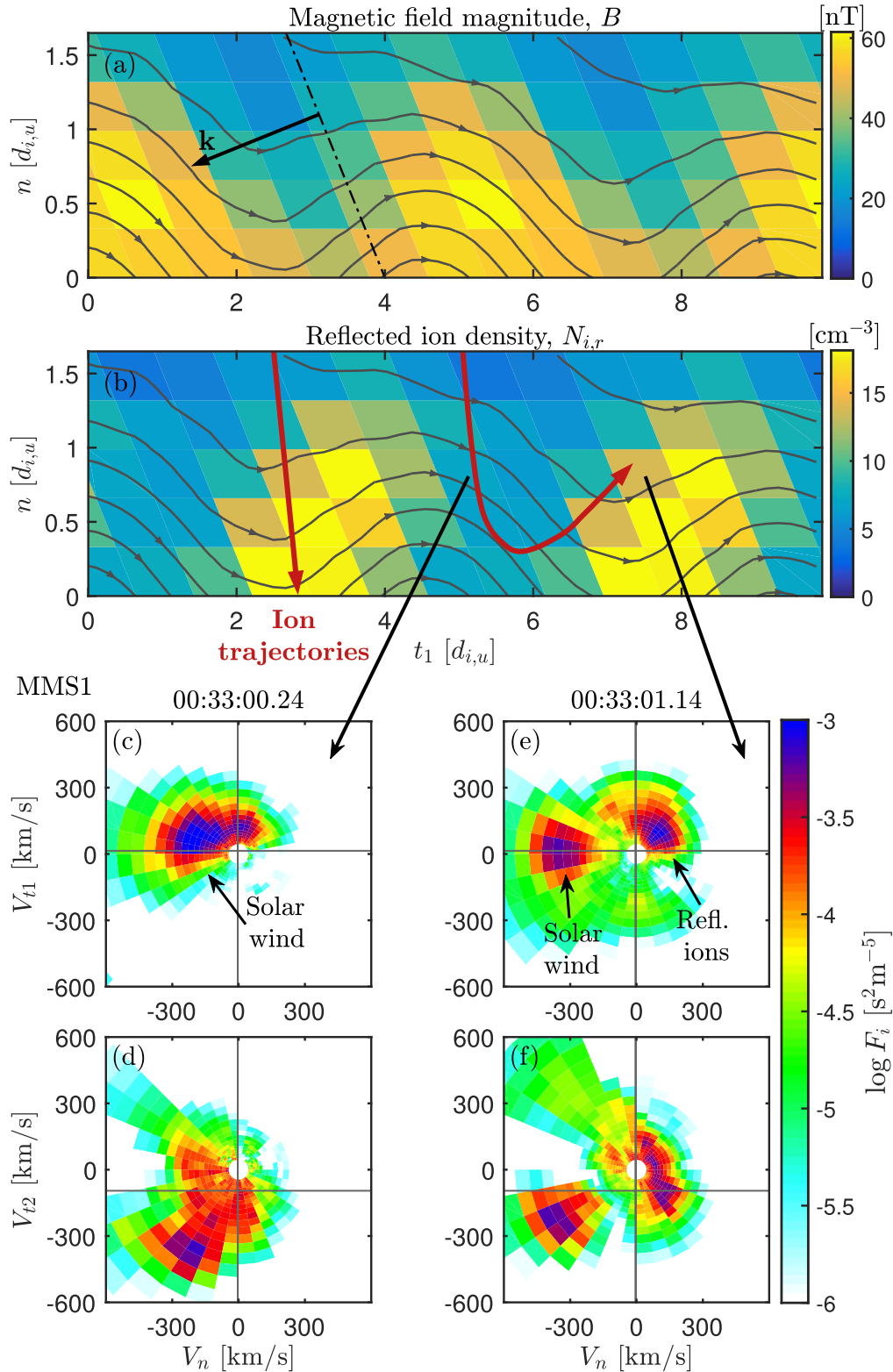
Figure 5. 2D histograms of the rippled shock compiled with data from all four spacecraft and representative ion distribution functions. (a) Magnetic field magnitude in the shock. Also shown are approximate field lines given from the magnetic field data. (b) Density of reflected ions. Two inferred ion trajectories for two incidence locations are shown as red arrows. (c)–(f) Projected ion distribution function, in two planes, for two times corresponding to different regions in the shock indicated by black arrows.

parameters, the whistler mode is damped. In addition, the frequency for whistler waves is higher and the observed waves are not clearly right-hand polarized as expected for whistler waves. The drift mirror mode has also been proposed

as the source of the ripples (Winske and Quest 1988). We note however that drift waves typically propagate perpendicular to both the density gradient and **B** (Goldston and Rutherford 1995), opposite to what is observed here where
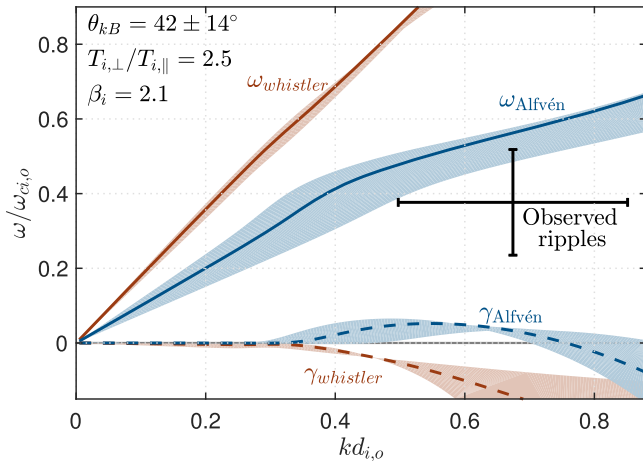
Figure 6. Dispersion relations for the lower and upper Alfvén wave mode from WHAMP and the observed ripples normalized to overshoot values. The solid lines show frequency and the dashed lines growth rate for the plasma parameters observed by MMS. Blue lines are for the Alfvén wave, red lines for the whistler branch. Error bars for the observations show the 2σ interval for k and ω and the shaded area show the 2σ interval for θ_{kB}. Uncertainties in the plasma and field measurements in the overshoot are omitted.

the waves are propagating in the coplanarity plane. Other factors that could help us differentiate between mirror and Alfvén waves like $B_\parallel$ fluctuations or compressibility are difficult to estimate due to the waves propagating in a strong gradient of magnetic field and density. We conclude that the ripples appear to fit the description of AIC waves although drift mirror waves cannot be entirely excluded.

When determining whether the shock was non-stationary due to ripples or self-reformation we made use of the Rankine–Hugoniot relations being locally fulfilled on the rippled shock. Such an assumption is approximate and requires validation. We can estimate the spatial amplitude of the ripples from figures 5(a), (b) or from the B_n fluctuations (Johlander *et al* 2016). In both cases we obtain a peak-to-peak amplitude $A \sim 30$ km, or $A/\lambda \sim 0.1$. If the ripples are sinusoidal in shape, this corresponds to a local change of $\hat{\mathbf{n}}$ of at most $\sim 17°$, in relatively good agreement with the $\sim 10°$ fluctuations required for the observed velocity fluctuations.

There are some questions about the shock ripples that this work does not answer. An open question about the shock ripples is that of direction of propagation. Here we find that the ripples propagate obliquely with a component anti-parallel to **B**, i.e. $\mathbf{k} \cdot \mathbf{B} < 0$. Most simulations are done with nearly perpendicular shocks (e.g. Winske and Quest 1988, Burgess *et al* 2016) and the ripples there propagate both parallel and anti-parallel to **B**. A recent simulation by Gingell *et al* (2017) with $\theta_{Bn} = 60°$ shows shock ripples propagating in the direction of **B**, contrary to the observations here. The difference in propagation direction can possibly be attributed to different sign of the upstream B_n, we observe $B_n < 0$, while the simulation has $B_n > 0$. The sign of B_n changes the guiding center motion of shock reflected ions in specular reflection (Schwartz *et al* 1983). It is possible this asymmetry could be linked to the propagation direction of the ripples. A

detailed instability analysis taking into account the shock reflected ions is outside the scope of this study and is left for future work. Another open question is about the electron dynamics at the rippled shock. In simulations by Umeda *et al* (2009), shock ripples are associated with increased electron acceleration through shock surfing acceleration. The questions concerning direction of propagation and electron acceleration are left for future work.

4. Conclusions

We have studied one crossing by the MMS spacecraft of the Earth's quasi-perpendicular and non-stationary bow shock. During the crossing MMS graze the shock ramp and overshoot for an unusually long time. Magnetic field and plasma measurements on MMS show large fluctuation throughout the shock crossing, indicating that the shock is non-stationary. The slow crossing, combined with the favorable inter-spacecraft distances of ~ 35 km, makes this event exceptionally well suited for studying ion-kinetic-scale fluctuations in the shock. Making use of multi-point observations and the high-cadence ion measurements, we conclude that the shock non-stationarity is in the form of ripples propagating along the shock surface.

The shock ripples are quasi-periodic fluctuations with a wave-like structure. Using timing and minimum variance analyzes, we accurately determined the dispersive properties of the ripples. We find that the ripples propagate in the coplanarity plane with an angle to the shock surface of $\sim 40°$ with $\mathbf{k} \cdot \mathbf{B} < 0$ and $\mathbf{k} \cdot \hat{\mathbf{n}} < 0$ and with a phase speed in the NI frame close to the local Alfvén speed. The frequency of the ripples is ~ 3 times the upstream ion gyrofrequency and the wavelength is ~ 5 upstream ion inertial lengths. Moreover the ripples are nearly linearly polarized with fluctuations mainly in the coplanarity plane, leading to an almost two-dimensional structure of the ripples. Overall, these dispersive properties are in good agreement with 2D and 3D kinetic simulations (e.g. Lowe and Burgess 2003, Burgess *et al* 2016).

We compared the observations of the shock ripples with a numerical dispersion solver, assuming linear waves in a homogeneous medium. The assumptions of linearity and homogeneity might be invalid for the shock ramp. Despite this, the ripples resemble AIC waves generated by an ion temperature anisotropy.

Detailed analysis of ion dynamics dependency on wave phase and distance to the shock revealed that ion reflection is localized to regions of the shock with higher magnetic field. This shows that ripples play an important role in ion dynamics at shocks in space.

Acknowledgments

ORCID iDs

Andreas Johlander ● https://orcid.org/0000-0001-7714-1870

References

Abraham-Shrauner B 1972 Determination of magnetohydrodynamic shock normals *J. Geophys. Res.* **77** 736

Blandford R D and Ostriker J P 1978 Particle acceleration by astrophysical shocks *Astrophys. J. Lett.* **221** L29–32

Burch J L, Moore T E, Torbert R B and Giles B L 2016 Magnetospheric multiscale overview and science objectives *Space Sci. Rev.* **199** 5–21

Burgess D, Hellinger P, Gingell I and Trávníček P M 2016 Microstructure in two- and three-dimensional hybrid simulations of perpendicular collisionless shocks *J. Plasma Phys.* **82** 905820401

Burgess D and Scholer M 2007 Shock front instability associated with reflected ions at the perpendicular shock *Phys. Plasmas* **14** 012108

Caprioli D, Pop A-R and Spitkovsky A 2015 Simulations and theory of ion injection at non-relativistic collisionless shocks *Astrophys. J. Lett.* **798** L28

Chanteur G 1998 Spatial interpolation for four spacecraft: theory *Analysis Methods for Multi-Spacecraft Data* (*ISSI Scientific Reports Series*) ed G Paschmann and P W Daly vol 1, 349–69

Davidson R C and Ogden J M 1975 Electromagnetic ion cyclotron instability driven by ion energy anisotropy in high-beta plasmas *Phys. Fluids* **18** 1045–50

Gingell I *et al* 2017 MMS observations and hybrid simulations of surface ripples at a marginally quasi-parallel shock *J. Geophys. Res.: Space Phys.* **122** 11,003–17

Goldston R J and Rutherford P 1995 *Introduction to Plasma Physics* (*Plasma Physics Series*) (Bristol: Institute of Physics Publishing)

Gosling J T and Thomsen M F 1985 Specularly reflected ions, shock foot thicknesses, and shock velocity determinations in space *J. Geophys. Res.* **90** 9893–6

Hao Y, Lu Q, Gao X and Wang S 2016 Ion dynamics at a rippled quasi-parallel shock: 2d hybrid simulations *Astrophys. J.* **823** 7

Hasegawa A 1969 Drift mirror instability of the magnetosphere *Phys. Fluids* **12** 2642–50

Hellinger P, Trávníček P, Lembège B and Savoini P 2007 Emission of nonlinear whistler waves at the front of perpendicular supercritical shocks: hybrid versus full particle simulations *Geophys. Res. Lett.* **34** L14109

Johlander A *et al* 2016 Rippled quasiperpendicular shock observed by the magnetospheric multiscale spacecraft *Phys. Rev. Lett.* **117** 165101

Krasnoselskikh V V, Lembège B, Savoini P and Lobzin V V 2002 Nonstationarity of strong collisionless quasiperpendicular shocks: theory and full particle numerical simulations *Phys. Plasmas* **9** 1192–209

Landau L D and Lifshitz E M 1960 *Electrodynamics of Continuous Media* (Oxford: Pergamon)

Lee K H 2017 Generation of parallel and quasi-perpendicular EMIC waves and mirror waves by fast magnetosonic shocks in the solar wind *J. Geophys. Res.: Space Phys.* **122** 7307–22

Lembege B, Giacalone J, Scholer M, Hada T, Hoshino M, Krasnoselskikh V, Kucharek H, Savoini P and Terasawa T 2004 Selected problems in collisionless-shock physics *Space Sci. Rev.* **110** 161–226

Lembège B and Savoini P 1992 Nonstationarity of a two-dimensional quasiperpendicular supercritical collisionless shock by self-reformation *Phys. Fluids* B **4** 3533–48

Lembège B and Savoini P 2002 Formation of reflected electron bursts by the nonstationarity and nonuniformity of a collisionless shock front *J. Geophys. Res.: Space Phys.* **107** 1037

Lembège B, Savoini P, Hellinger P and Trávníček P M 2009 Nonstationarity of a two-dimensional perpendicular shock: Competing mechanisms *J. Geophys. Res.: Space Phys.* **114** A03217

Lobzin V V, Krasnoselskikh V V, Bosqued J-M, Pinçon J-L, Schwartz S J and Dunlop M 2007 Nonstationarity and reformation of high-Mach-number quasiperpendicular shocks: Cluster observations *Geophys. Res. Lett.* **34** L05107

Lowe R E and Burgess D 2003 The properties and causes of rippling in quasi-perpendicular collisionless shock fronts *Ann. Geophys.* **21** 671–9

Matsukiyo S and Matsumoto Y 2015 Electron acceleration at a high beta and low mach number rippled shock *J. Phys.: Conf. Ser.* **642** 012017

McKean M E, Omidi N and Krauss-Varban D 1995 Wave and ion evolution downstream of quasi-perpendicular bow shocks *J. Geophys. Res.* **100** 3427–37

Morlino G and Caprioli D 2012 Strong evidence for hadron acceleration in Tycho's supernova remnant *Astron. Astrophys.* **538** A81

Moullard O, Burgess D, Horbury T S and Lucek E A 2006 Ripples observed on the surface of the Earth's quasi-perpendicular bow shock *J. Geophys. Res.: Space Phys.* **111** A09113

Ofman L and Gedalin M 2013 Rippled quasi-perpendicular collisionless shocks: local and global normals *J. Geophys. Res.: Space Phys.* **118** 5999–6006

Ogilvie K W *et al* 1995 SWE, a comprehensive plasma instrument for the wind spacecraft *Space Sci. Rev.* **71** 55–77

Pollock C *et al* 2016 Fast plasma investigation for magnetospheric multiscale *Space Sci. Rev.* **199** 331–406

Rönnmark K 1982 WHAMP - Waves in homogeneous, anisotropic, multicomponent plasmas *Report* 179 Kiruna Geophysical Institute

Russell C T *et al* 2016 The magnetospheric multiscale magnetometers *Space Sci. Rev.* **199** 189–256

Saito S and Umeda T 2011 Suppression of reflected electrons by kinetic alfvén turbulence in a quasi-perpendicular shock: particle-in-cell simulations *Astrophys. J.* **736** 35

Schwartz S J 1998 Shock and discontinuity normals, mach numbers, and related parameters *Analysis Methods for Multi-Spacecraft Data* (*ISSI Scientific Reports Series*) ed G Paschmann and P W Daly vol 1, 249–70

Schwartz S J and Burgess D 1991 Quasi-parallel shocks—a patchwork of three-dimensional structures *Geophys. Res. Lett.* **18** 373–6

Schwartz S J, Thomsen M F and Gosling J T 1983 Ions upstream of the Earth's bow shock—a theoretical comparison of alternative source populations *J. Geophys. Res.* **88** 2039–47

Slavin J A and Holzer R E 1981 Solar wind flow about the terrestrial planets: I. Modeling bow shock position and shape *J. Geophys. Res.* **86** 11401–18

Sonnerup B U Ö and Scheible M 1998 Minimum and maximum variance analysis *ISSI Sci. Rep. Ser.* **1** 185–220

Tsurutani B T and Stone R G 1985 *Collisionless Shocks in the Heliosphere: Reviews of Current Research* (Washington, DC: American Geophysical Union) p 35

Umeda T, Yamao M and Yamazaki R 2009 Electron acceleration at a low mach number perpendicular collisionless shock *Astrophys. J.* **695** 574–9

Vogt J, Haaland S and Paschmann G 2011 Accuracy of multi-point boundary crossing time analysis *Ann. Geophys.* **29** 2239–52

Winske D and Quest K B 1988 Magnetic field and density fluctuations at perpendicular supercritical collisionless shocks *J. Geophys. Res.* **93** 9681–93

Yang Z W, Lembège B and Lu Q M 2012 Impact of the rippling of a perpendicular shock front on ion dynamics *J. Geophys. Res.: Space Phys.* **117** A07222

Yang Z W, Lu Q M, Lembège B and Wang S 2009 Shock front nonstationarity and ion acceleration in supercritical perpendicular shocks *J. Geophys. Res.: Space Phys.* **114** A03111